Journal of Solid Mechanics Vol. 9, No. 3 (2017) pp. 587-598

Predicting Depth and Path of Subsurface Crack Propagation at Gear Tooth Flank under Cyclic Contact Loading

H. Heirani, Kh. Farhangdoost *

Mechanical Engineering Department, Faculty of Engineering, Ferdowsi University of Mashhad, Mashhad, Iran

Received 22 June 2017; accepted 20 August 2017

ABSTRACT

In this paper, a two-dimensional computational model is proposed for predicting the initiation position and propagation path of subsurface crack of spur gear tooth flank. In order to simulate the contact of teeth, an equivalent model of two contacting cylinders is used. The problem is assumed to be under linear elastic fracture mechanic conditions and finite element method is used for numerical study. An initial subsurface crack is considered in the model at different depths. For each position of the initial crack, moving contact loading is applied to the part and value of ΔK_{II} is obtained for the crack tips. The position of maximum ΔK_{II} is selected as the location of crack initiation. It is shown that the subsurface crack appears at the maximum shear stress point. The maximum tangential stress criterion is used to determine the crack growth angle. The crack is incrementally propagated until the crack tip reaches the part surface and a cavity is formed on the tooth surface. Analyzing the stress field and stress intensity factors are performed in ABAQUS software. The obtained results for the depth and shape of the spall are in good agreement with the experimental results reported in literature.

Keywords: Spalling; Crack initiation and propagation; Gear; Finite element; Fatigue.

1 INTRODUCTION

SOME parts in most mechanical machinery are in contact together. These parts may be stationary or in relative movement. When these mechanical components undergo loading, significant compressive stress is generated at their contact areas. Gears, rolling bearings, wheel and railway, clutches, brakes, screws, and rivet joints are among the most important parts [1]. When the contacting parts are in relative movement, contact stresses will be cyclic due to the change of contact area position during the moving period. In the presence of cyclic loading, fatigue phenomenon occurs. Contact fatigue is a type of damage made by changes in the material microstructure. Contact fatigue leads to crack initiation at first and then induces crack propagation.

Gears are among the most important parts of machines. Since gears transmit the motion and power by the contact of surfaces, the gears performance depends on the conditions of teeth surfaces. In gear practice pitting, scoring and tooth breakage constitute the major catastrophic failures [2,3]. Generally, there are four fundamental wear modes: contact fatigue, adhesion, abrasion, and corrosion [4]. Under normal operating conditions, contact fatigue is the most conventional failure mode on gear tooth surface.

Surface contact fatigue was first studied by Way in 1935 [5] via pitting experiment. After that, researchers have focused on this phenomenon. Previous works on surface contact fatigue can be classified into two groups in terms of crack position: surface cracks and subsurface cracks. Some studies have investigated crack initiation [6-11], some have considered crack propagation [12-19], and others have focused on both [20-23].

*Corresponding author. Tel.: +98 513 880 5059; Fax: +98 513 876 3304.
E-mail address: farhang@um.ac.ir (Kh. Farhangdoost).

Sraml et al. [6,7] presented computational models for the simulation of contact fatigue-damage initiation in the contact area of meshing gears. These models are based on the Coffin-Manson relationship between deformations and loading cycles. Alfredsson et al. [8,23,24] numerically investigated the effect of contact loading of a surface irregularity, i.e. asperity. They found that asperities increase stress in contact area. They represent the point loading mechanism caused by asperity as a source of the rolling contact fatigue started from the surface.

There have been numerous studies on the life and path of surface crack growth [14,15,18,19,22]. In all of these works, the part has been assumed to have an initial surface crack and the effect of lubricant film has also been studied. Fluid trapped in the crack leads to its growth as a result of tensile mode loading. Virtual crack extension and minimum strain energy density methods have been applied to investigate crack propagation. In subsurface crack investigations the lubricant film is not considered because of no fluid trapped in the crack.

In other studies, researchers have studied the initiation and propagation of subsurface cracks. Beheshti and Khonsari [10] applied the principles of continuum damage mechanics to predict the life and the initiation point of rolling and sliding contact fatigue crack. This approach included estimating subsurface stresses and damage state in contact area. They didn't investigate crack propagation. Glodez et al. [12,13,17,20,21] considered the initial subsurface crack at the maximum von Mises stress point and analyzed the crack propagation based on mode I stress intensity factor, but since the mode *I* stresses are compressive, in contact loading, crack initiation and propagation cannot occur just by mode *I*. Aslantas and Tasgetiren [16] conducted a numerical and experimental study on the life and path of subsurface crack growth. They also considered an initial crack at maximum von Mises stress point and used maximum tangential stress criterion to determine the crack growth direction. They assumed that crack grows from one tip, but in this study it is shown that stress intensity factors are equal at both initial subsurface crack tips. However, by conducting a numerical and experimental research, Ding and Gear [9] showed that shear stress is the cause of the initiation of subsurface crack under contact loading. They proposed ligament collapse model as the mechanism of the spalling formation on the gear tooth flank.

The cavity on the gear tooth flank due to contact fatigue loading can be divided into two general types: pitting and spalling. Pitting appears as shallow craters on contact surfaces with the maximum depth of 10 μm. Spalling is made as deeper cavities with the depth within the range of 20-100 μm [9]. Pitting and spalling are generated by the propagation of surface and subsurface cracks, respectively. Due to larger size and more important role of spalling in the damage of tooth surface, it is necessary to examine this phenomenon.

Previous studies on subsurface crack have assumed that the initial crack appears at the maximum von Mises stress point, except [9]. Ding and Gear [9] demonstrated that, during contact loading, shear stress causes the initiation of subsurface crack. Some studies have investigated crack initiation and propagation based on maximum mode *I* stress intensity factor, K_I. Since the mode *I* leads to compressive stresses in contact loading, no crack initiation and propagation occur in this mode; however, they would appear in the mode *II* loading. Moreover, all the previous studies assumed that crack propagation continues from one tip to part surface and, after reaching the surface, another tip is allowed to grow. In previous studies, after determining the width of contact area and maximum contact pressure using Hertz contact theory, the same moving parabolic load distribution was used at the contact surface. In this study, it is tried to make this problem closer to the real conditions and present a modified model.

In this study, spalling formation on the tooth surface is investigated. When a part undergoes cyclic contact loading, after some specific numbers of cycles, cracks are initiated in the part or the initial defects of the part and are activated. For three samples, locations of maximum shear, Tresca, and von Mises stresses are compared with the experimental spalling depth to propose the initiation location of subsurface crack. It is assumed that crack propagates in the mixed mode *I/II* loading. After the crack initiation, crack is grown from both tips in the following cycles of loading until the crack tip reaches the part surface. Then, a piece of the material is cut from the part and a spall is formed on the gear tooth surface. Furthermore, complete contact of two cylinders is considered for all the crack propagation steps in order to take into account the probable variations of pressure distribution profile due to the strength variation caused by crack growth in the part. Finally, the results obtained from the proposed model are compared with the experimental results of other literature.

2 NUMERICAL SIMULATIONS

2.1 Contact analysis

As the contacting tooth moves up the profile of the loaded tooth, a sliding-rolling action takes place at the profile interface. At the pitch line, the stresses are pure rolling. At the same time, there is a tensile stress at the root radius of the loaded side of the tooth. Fig. 1 shows the loading on different regions of flank tooth [25]. Experimental results of

literature [9,19,23,26,27] prove that initiation and propagation of surface and subsurface cracks can occur on the pitch line region, therefore this paper focuses on the subsurface cracks subjected to contact loading, and this loading is maximized on the pitch point.

Problem of contact between two gear teeth can be simplified using two cylinders with the equivalent curvature radius of the contact point of teeth (Fig. 2) [6-8,12-18,20-23]. According to Hertz theory, when two cylinders of length l and diameters d_1 and d_2 are compressed against each other by force F, the contact line between them is transformed into a rectangular-shaped area with the width of $2b$ [28]:

$$b = \sqrt{\frac{2F}{\pi l}\frac{1-\nu_1^2 \Big/ E_1 + 1-\nu_2^2 \Big/ E_2}{1/d_1 + 1/d_2}} \tag{1}$$

d_1 and d_2 are the diameters of the flank tooth involute profile at any contact point. In this paper, fatigue crack propagation is investigated in a short region length (0.4 *mm*) around the pitch point where contact pressure is maximized. In most of previous studies [6-8,12-18,20-23], curvature radius was selected constant during the simulation.

As a result of this loading, a parabolic pressure distribution is made on the contact area, whose maximum value at the contact surface would be [28]:

$$p_{\max} = \frac{2F}{\pi b l} \tag{2}$$

In previous studies, after determining the width of contact area and maximum contact pressure using Hertz contact theory, the same moving parabolic load has been used at the flat contact surface to analyze the problems [6,7,13,14,16,20-22]. In this study, a moving contact cylinder was considered instead of a parabolic load, in order to take into account the probable variations of pressure distribution profile due to the strength variation caused by subsurface crack growth.

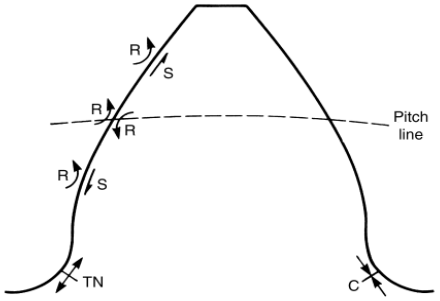

Fig.1
The loading on different regions of flank tooth [25].

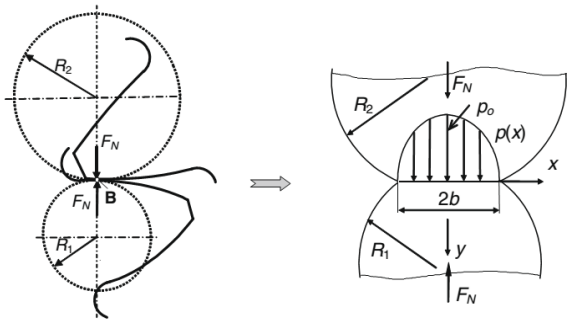

Fig.2
Equivalent contact model of two cylinders instead of the gear teeth.

2.2 Finite element model

There are complex relations in contact mechanics and fracture mechanic. Theoretical analysis of the fatigue crack initiation and propagation in the parts undergoing contact loading is very hard or sometimes impossible to analyze

because of involving both contact mechanics and fracture mechanics, simultaneously. To solve such problems, finite element method is strongly efficient and has been widely used. In this study, ABAQUS software is used to determine the stress field distribution and the mode *I* and mode *II* stress intensity factors. The material model is assumed to be elastic and homogeneous.

The geometry of the problem, as shown in Fig. 3, which has an initial subsurface crack, is modeled by ABAQUS software. Initial cracks of length 15, 20, and 50 μm have been considered in the literature [13, 14, 16, 17, 19-22]. In this study, an initial subsurface crack of length 20 μm is considered. The subsurface crack is placed at different depths (H). *CPE4R* and *CPE6M* plane strain elements are employed to mesh the parts and crack tip region, respectively [29]. The crack is defined as contour integral to present stress intensity factors, K_I and K_{II}, in the output. One part is fixed in two directions and another part is moved on the first part surface to apply a loading cycle on the crack tips. The problem is simulated in static general mode. The friction coefficient is very small (f<0.06) [4,9,30] in suitable lubricating conditions of gears. In inappropriate lubricating conditions and large friction coefficient, initial cracks generally appear on the material surface, which cause pitting. For small friction coefficients and completely smooth contact surfaces, cracks are initiated below the surface layer or subsurface defects are activated and cause spalling formation [31]. It is experimentally illustrated in the literature [12,13,16,21] that subsurface cracks can initiate and propagate under the contact loading conditions. Since spalling formation is investigated in this study, the assumptions of good surface finishing, appropriate lubricating conditions and frictionless contact are considered.

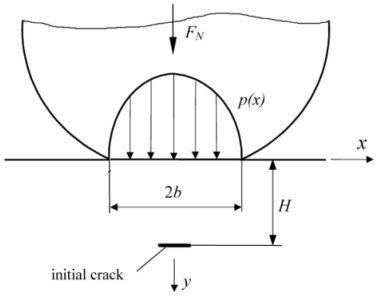

Fig.3
Position of initial subsurface crack along with the applied force to the surface.

3 RESULTS AND DISCUSSION

3.1 Fatigue crack initiation

In most of the previous studies, location of maximum von Mises stress is considered as the initiation crack place. In contact fatigue loading, subsurface cracks are subjected to mode *I* and mode *II* loading, simultaneously. Since the mode *I* loading is compressive and compressive load cannot induce crack propagation, the cause of subsurface crack initiation and propagation will be shear load and mode *II* loading. Ding and Gear [9] showed that, in contact fatigue loading, shear stress causes subsurface crack initiation. In this study, for three contact loading samples, components of the shear, von Mises, and Tresca stresses were calculated at different depths. Moreover, for each sample, an initial crack is placed at different depths of the surface and stress intensity factors are calculated for the crack tips. Three experimental samples are selected from literature [4,9,21] and presented in Table 1.

Table 1
Characteristics of three sample experimental studies selected for the analysis.

Case	Part	$E_1=E_2$ (GPa)	$\nu_1=\nu_2$	R^* (mm)	P_{max} (MPa)	K_{Ic} $(MPa.m^{0.5})$
a	Steel gears [4,9]	195	0.3	3.7	1885	57 [32]
b	Steel gears [4,9]	195	0.3	3.7	1503	57 [32]
c	42CrMo4 cylinders [21]	206	0.3	10	1550	63-95

R^* is the equivalent radius of contact pair, defined as $R^* = (R_1R_2)/(R_1+R_2)$ [33]. In case a and b pitch diameter of pinion and gear are d_p=38.1 mm and d_g=50.8 mm, respectively [4].

In this section, the contact stress components, calculated by the ABAQUS software for different mesh sizes of sample *a*, are shown in Fig. 4 to determine appropriate mesh size and show independence of results from mesh size. According to Fig. 4, the results are independent of mesh size for the mesh of length 1 μm. Therefore, 1 μm mesh size is used at the contact area and crack tip region.

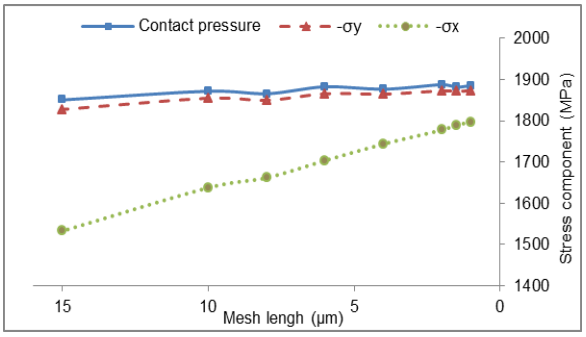

Fig.4
Effect of mesh size on contact stress components (sample *a*).

Figs. 5-7 show variations of the components of the shear, von Mises, and Tresca stresses for samples *a*, *b* and *c* in terms of depth from surface. Loading is static and stresses are calculated beneath the contact surface. Figs. 5-7 show that all three stress components have an increasing behavior at first; then, they show a decreasing trend. Each stress component is maximized at a specific depth.

Afterwards, an initial crack is placed at different depths from the surface, as shown in Fig. 3. The load is moved on the contact surface. The position of the load is shown with "*d*" which is the distance between the center of the initial crack and the contact point (Fig. 8). The value of stress intensity factors in the right and left crack tips is computed in several steps using ABAQUS software. For each depth, value of $\Delta K_{II} = K_{II,max} - K_{II,min}$ is calculated. After displacing the location of initial crack and determining ΔK_{II} several times, the depth generating maximum value of ΔK_{II} is selected. Fig. 9 shows the variations of ΔK_{II} in terms of the initial crack depth from the surface for sample c as an example.

In previous studies, different locations were considered as the place of initial subsurface crack, which include the location of maximum Tresca stress [6,7], maximum von Mises stress [12,13,16,17,20,21], and maximum shear stress [4,9]. To propose a model describing the initiation location of subsurface crack, the obtained depth of spalls on the steel gear flank from experiments [4,9,21], as shown in Fig. 10, is compared with depth of maximum ΔK_{II} ($K_{II,max}$-$K_{II,min}$), shear, Tresca, and von Mises stresses. Table 2. shows the results related to the depth of stress components and spalls.

Table 2
Depth of maximum stress components and spalls for three sample models.

Case	Shear stress (μm)	ΔK_{II} (μm)	von Mises (μm)	Tresca (μm)	Spall depth (experiment) (μm)
a	51	51	72	81	52 [9]
b	40	40	57	64	37 [9]
c	142	142	202	224	≈ 150 [21]

Results in Table 2. prove that the location of maximum shear stress, i.e. location of maximum value of ΔK_{II}, has the highest correspondence with the location of spall bottom. Therefore, in this model, position of maximum shear stress, maximum ΔK_{II}, is proposed as the initiation location of subsurface crack or activation of material defects. This recommendation is in agreement with Ding and Gear hypothesis [9] that shear stress governs the initiation of subsurface crack in the parts undergoing contact fatigue loading.

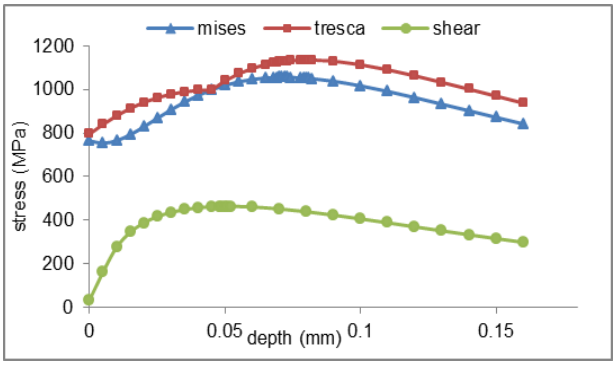

Fig.5
Variations of stress components in terms of depth from the surface for sample *a*.

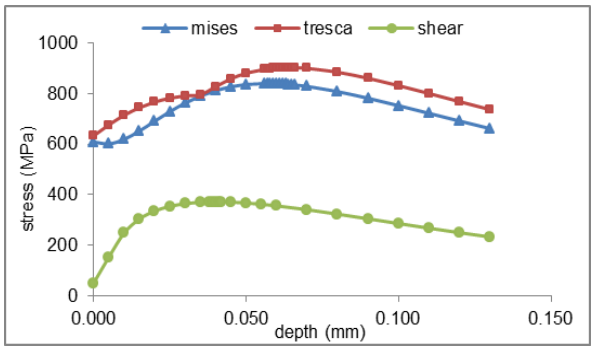

Fig.6
Variations of stress components in terms of depth from the surface for sample *b*.

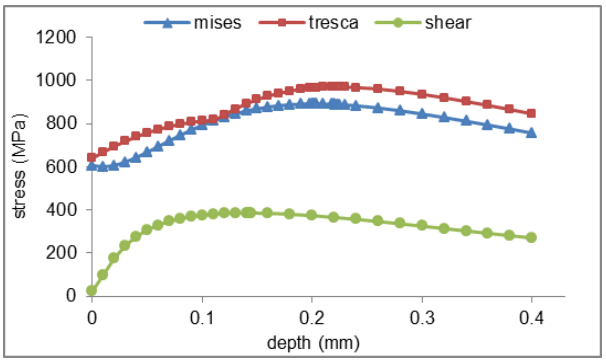

Fig.7
Variations of stress components in terms of depth from the surface for sample *c*.

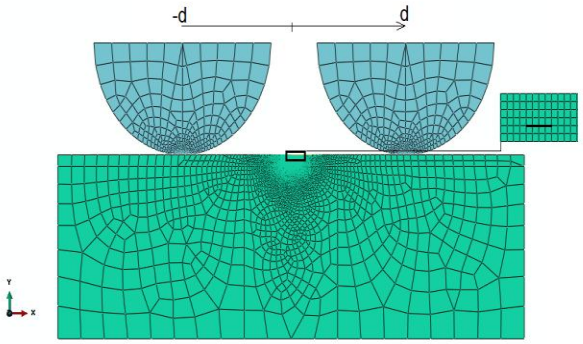

Fig.8
Movement of contact above the crack region.

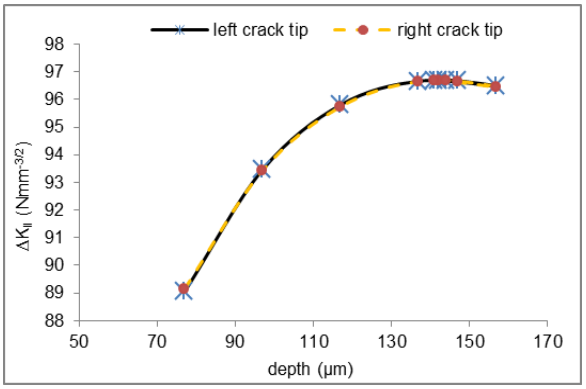

Fig.9
Variations of ΔK_{II} in terms of depth of initial crack from the surface in sample *c*.

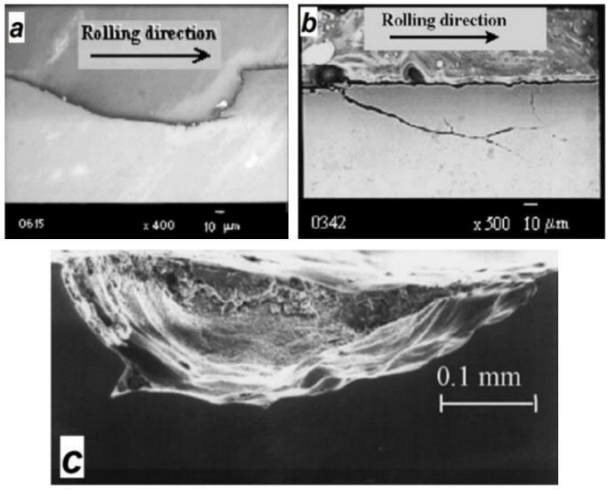

Fig.10
Spalls made on the gear teeth surface for three samples a, b [9], and c [21].

3.2 Fatigue crack propagation

After determining the location of initial subsurface crack, mechanism and path of crack propagation are investigated. Since stress distribution at the crack tip determines the mechanism of crack propagation, it is essential to investigate stress fields at the crack tip. Fig. 11 shows the stress field in 2D problems with crack. In plane mixed mode problems, mixed mode *I/II*, stress field of the crack tip is as follows [34]:

$$\sigma_r = \frac{K_I}{4\sqrt{2\pi r}}\left[5\cos\left(\frac{\theta}{2}\right)-\cos\left(\frac{3\theta}{2}\right)\right]-\frac{K_{II}}{4\sqrt{2\pi r}}\left[5\sin\left(\frac{\theta}{2}\right)-3\sin\left(\frac{3\theta}{2}\right)\right] \tag{3}$$

$$\sigma_\theta = \frac{K_I}{4\sqrt{2\pi r}}\left[3\cos\left(\frac{\theta}{2}\right)+\cos\left(\frac{3\theta}{2}\right)\right]-\frac{K_{II}}{4\sqrt{2\pi r}}\left[3\sin\left(\frac{\theta}{2}\right)+3\sin\left(\frac{3\theta}{2}\right)\right] \tag{4}$$

$$\tau_{r\theta} = \frac{K_I}{4\sqrt{2\pi r}}\left[\sin\left(\frac{\theta}{2}\right)+\sin\left(\frac{3\theta}{2}\right)\right]+\frac{K_{II}}{4\sqrt{2\pi r}}\left[\cos\left(\frac{\theta}{2}\right)-3\cos\left(\frac{3\theta}{2}\right)\right] \tag{5}$$

where r is the distance from the crack tip, θ is angle relative to crack direction, K_I and K_{II} are the mode *I* and mode *II* stress intensity factors, and σ_r, σ_θ, and $\tau_{r\theta}$ are radial, tangential, and shear components of stress, respectively.

The crack growth path is determined according to Erdogan-Sih crack growth prediction criterion [35]. This criterion is based on maximum tangential stress, σ_θ, for plane mixed mode problems. According to this criterion, the crack grows in a radial direction from its tip and with the angle of $\theta = \theta_0$, which is perpendicular to the maximum tangential stress, $\sigma_{\theta,max}$. Maximum value of tangential stress occurs where the derivative of this stress component to θ is zero.

In the subsurface crack subjected to contact fatigue loading, stress intensity factor K_{II} has both negative and positive values. According to the maximum tangential stress criterion, positive value of K_{II} deviates the crack away from the contact surface, while the negative value deviates it toward the contact surface (Fig. 12).

$$\left.\frac{\partial\sigma_\theta}{\partial\theta}\right|_{\theta=\theta_0} = 0, \quad \left.\frac{\partial^2\sigma_\theta}{\partial\theta^2}\right|_{\theta=\theta_0} \prec 0 \tag{6}$$

$$\begin{aligned}\left.\frac{\partial\sigma_\theta}{\partial\theta}\right|_{\theta=\theta_0} &= \frac{K_I}{4\sqrt{2\pi r}}\left[-\frac{3}{2}\sin\left(\frac{\theta_0}{2}\right)-\frac{3}{2}\sin\left(\frac{3\theta_0}{2}\right)\right]-\frac{K_{II}}{4\sqrt{2\pi r}}\left[\frac{3}{2}\cos\left(\frac{\theta_0}{2}\right)+\frac{9}{2}\cos\left(\frac{3\theta_0}{2}\right)\right]\\ \left.\frac{\partial\sigma_\theta}{\partial\theta}\right|_{\theta=\theta_0} &= 0 \Rightarrow K_I\left[\sin\left(\frac{\theta_0}{2}\right)+\sin\left(\frac{3\theta_0}{2}\right)\right]+K_{II}\left[\cos\left(\frac{\theta_0}{2}\right)+3\cos\left(\frac{3\theta_0}{2}\right)\right]=0\end{aligned} \tag{7}$$

$$\theta_0 = -\cos^{-1}\left(\frac{3K_{II}^2 + K_I\sqrt{K_I^2+8K_{II}^2}}{K_I^2+9K_{II}^2}\right) \quad (8)$$

In the first step, an initial crack is considered at the depth corresponding to the maximum value of ΔK_{II}, which is assumed as the initiation location of subsurface crack. Contact of the two parts happens at the point before the crack and is moved on the contact surface. By moving the contact load on the surface and applying a loading cycle, the mode *I* and mode *II* stress intensity factors for both of crack tips are calculated by ABAQUS software. Stress intensity factors are converged in 2 or 3 contours and in this study converged results are represented and used. Moving contact loading is simulated in quasi-static form. Figs. 13 and 14 show the variations of the mode *I* and mode *II* stress intensity factors for the initial crack in terms of load distance from the crack center, *d* (see Fig. 8), in sample *a*, respectively. Due to reversal shear stress under the surface, the mode *II* stress intensity factor increases to a positive maximum value and then decreases to a negative minimum value.

ΔK_{th} of most of steels is less than 8 $MPa.m^{0.5}$ [36], initial crack length and loading magnitude of this study create $\Delta K_{eq}= (\Delta K_I^4+8\Delta K_{II}^4)^{1/4}$ [37] higher than ΔK_{th}, so by these assumptions fatigue crack growth can occur.

After determining the mode *I* and mode *II* stress intensity factors, angle of crack propagation can be calculated by Eq. (8). In the next step, the crack is incrementally grown in the direction of the obtained angle and stress intensity factors are determined. In each step, the mode *I* and mode *II* stress intensity factors are obtained by modeling and solving the problem using ABAQUS software and crack growth angle is also determined. Since, for the initial crack, ΔK_{II} value for both right and left crack tips is equal, when ΔK_{II} reaches the threshold value, crack growth starts from both tips. In some previous works [12,13,16,17,20,21], subsurface crack has been extended from only one tip and, after reaching the contact surface, crack growth has been started from another tip, which does not seem to be true. Figs. 15 and 16 display the variations of ΔK_{II} for left and right crack tips in sample *a* during different incremental crack growth steps, respectively. Step 1 indicates an initial subsurface crack and subsequent steps indicate cracks after incremental growth. In these steps, $K_{eq}= (K_I^4+8K_{II}^4)^{1/4}$ [37] is less than K_{Ic}.

After some steps of incremental crack propagation, the right tip changes its direction toward the part center; but the left tip changes its direction toward the part surface during all the steps until reaches the surface. In the next loading cycle, the piece of the material below which the crack is formed, acts like a cantilever beam. In case tensile stresses at the surface are larger than the ultimate strength of material, a new sudden fracture would happen from the contact surface to the crack. Thus, a spall is formed on the tooth surface. Fig. 17 shows several incremental steps of crack growth, from initial subsurface crack to the spalling formation, for sample a according to the model proposed in this study.

For two samples *a* and *b*, spalling formation steps, from initiation subsurface crack to cavity formation on the contact surface, are studied. The spalls formed by the proposed model are shown in Fig. 18 and compared with the experimental results of spalling formation on the steel gear flank from literature. Fig. 18 shows a good agreement between the results obtained from the proposed model and the experimental ones [4,9].

Two samples *a* and *b* have similar materials and geometry, but they are subjected to different loads. Table 2. shows spalling of sample *a* is deeper than spalling of sample *b*. Also, Fig. 18 shows that sample *a* has a larger spalling than sample *b*, because sample *a* is subjected to greater load and maximum contact pressure than sample *b*.

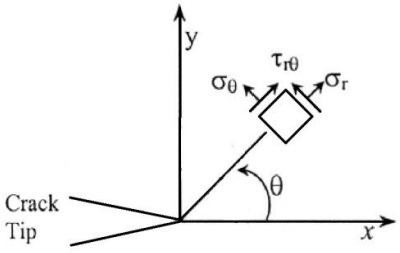

Fig.11
Stress field at two-dimensional crack tip.

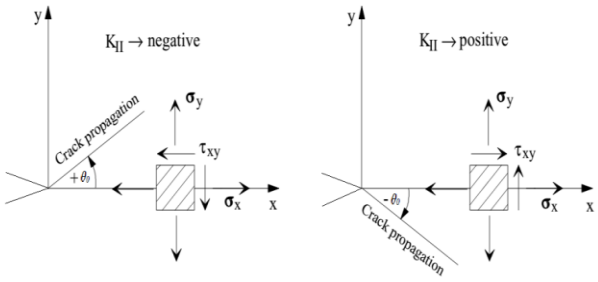

Fig.12
Variation of the angle of crack direction undergoing plane mixed mode loading.

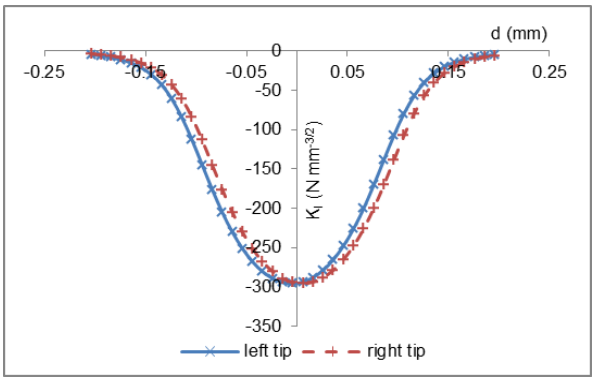

Fig.13
Variations of K_I in terms of load distance from the crack center for initial crack of sample *a*.

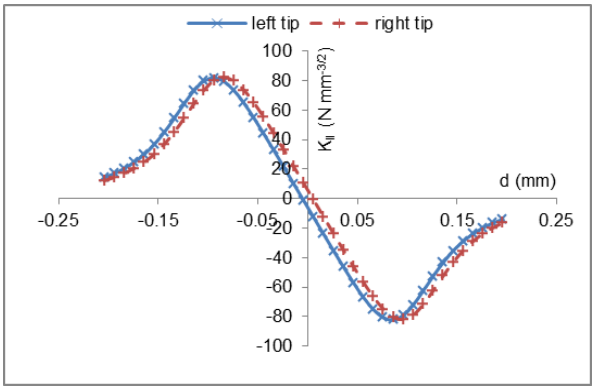

Fig.14
Variations of K_{II} in terms of load distance from the crack center for initial crack of sample *a*.

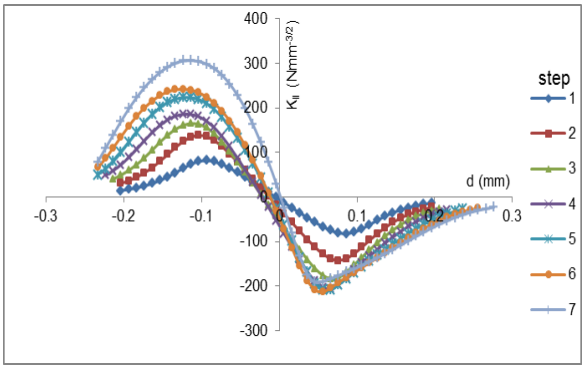

Fig.15
Variations of K_{II} for left crack tip in terms of load distance from center of the initial crack for different incremental steps of the crack growth in sample *a*.

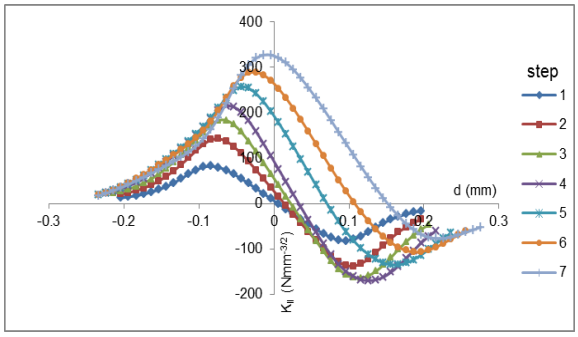

Fig.16
Variations of K_{II} for right crack tip in terms of load distance from center of the initial crack for different incremental steps of the crack growth in sample *a*.

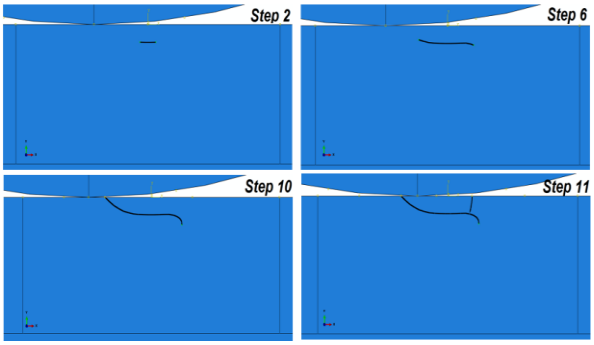

Fig.17
Several incremental steps of the subsurface crack propagation, from initial subsurface crack to spalling formation, for sample *a*.

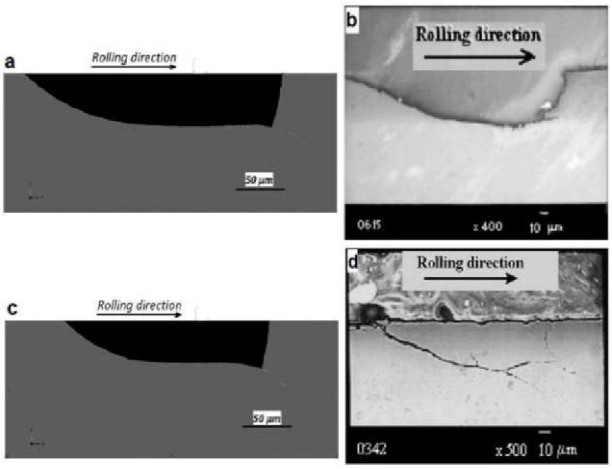

Fig.18
Shape and dimensions of spall formed in: a. simulation of sample *a,* b. experiment for sample *a* [9], c. simulation of sample *b*, and d. experiment for sample *b* [9].

4 CONCLUSIONS

Contact fatigue cracks are among the most conventional causes of gear damage. There are two types of contact fatigue cracks: surface cracks and subsurface cracks. A computational model for predicting the initiation and propagation of subsurface crack subjected to contact fatigue loading was proposed according to linear elastic fracture mechanics.

Position of maximum ΔK_{II} as well as shear, Tresca, and von Mises stresses are obtained for some samples using finite element analysis and the results are compared with the depth of experimental spalls. It is concluded that the model for predicting the initiation point of subsurface crack and spall depth is based on maximum ΔK_{II} and shear stress. This model proposed maximum shear stress as the criterion for subsurface crack initiation.

The crack is incrementally propagated with the angle obtained by Erdogan-Sih criterion. This model proposed mixed mode *I/II* as the criterion for subsurface crack propagation. Initial subsurface crack grows from both tips. It is

supposed that if one crack tip reached the contact surface, upper region of the crack would meet a sudden fracture. The fracture follows to the crack line and thus a spall is formed at the contact surface. The shape of the spalls predicted by the proposed model is in good agreement with the experimental results reported in literature.

REFERENCES

[1] Boresi A.P., Schmidt R.J., Sidebottom O.M., 1993, *Advanced Mechanics of Materials*, John wiley & sons, Hoboken.

[2] Spitas V., Spitas C., 2007, Numerical and experimental comparative study of strength-optimised AGMA and FZG spurgears, *Acta Mechanica* **193**: 113-126.

[3] Spitas C., Spitas V., Amani A., Rajabalinejad M., 2014, Parametric investigation of the combined effect of whole depth and cutter tip radius on the bending strength of 20◦ involute gear teeth, *Acta Mechanica* **225**: 361-371.

[4] Ding Y., Rieger N.F., 2003, Spalling formation mechanism for gears, *Wear* **254**: 1307-1317.

[5] Way S., 1935, Pitting due to rolling contact, *Journal of Applied Mechanics, Transactions of ASME* **57**: A49-A58.

[6] Sraml M., Flasker J., Potrc I., 2003, Numerical procedure for predicting the rolling contact fatigue crack initiation, *International Journal of Fatigue* **25**: 585-595.

[7] Sraml M., Flasker J., 2007, Computational approach to contact fatigue damage initiation analysis of gear teeth flanks, *International Journal of Advanced Manufacturing Technology* **31**: 1066-1075.

[8] Alfredsson B., Dahlberg J., Olsson M., 2008, The role of a single surface asperity in rolling contact fatigue, *Wear* **264**: 757-762.

[9] Ding Y., Gear J.A., 2009, Spalling depth prediction model, *Wear* **267**: 1181-1190.

[10] Beheshti A., Khonsari M.M., 2011, On the prediction of fatigue crack initiation in rolling/sliding contacts with provision for loading sequence effect, *Tribology International* **44**: 1620-1628.

[11] Moorthy V., Shaw B.A.,2013, An observation on the initiation of micro-pitting damage in as-ground and coated gears during contact fatigue, *Wear* **297**: 878-884.

[12] Glodez S., Winter H., Stuwe H.P., 1997, A fracture mechanics model for the wear of gear flanks by pitting, *Wear* **208**: 177-183.

[13] Glodez S., Ren Z., 1998, Modelling of crack growth under cyclic contact loading, *Theoretical and Applied Fracture Mechanics* **30**: 159-173.

[14] Flasker J., Fajdiga G., Glodez S., Hellen T.K., 2001, Numerical simulation of surface pitting due to contact loading, *International Journal of Fatigue* **23**: 599-605.

[15] Ren Z., Glodez S., Fajdiga G., Ulbin M., 2002, Surface initiated crack growth simulation in moving lubricated contact, *Theoretical and Applied Fracture Mechanics* **38**: 141-149.

[16] Aslantas K., Tasgetiren S., 2004, A study of spur gear pitting formation and life prediction, *Wear* **257**: 1167-1175.

[17] Glodez S., Abersek B., Flasker J., Ren Z., 2004, Evaluation of the service life of gears in regard to surface pitting, *Engineering Fracture Mechanics* **71**: 429-438.

[18] Fajdiga G., Flasker J., Glodez S., 2004, The influence of different parameters on surface pitting of contacting mechanical elements, *Engineering Fracture Mechanics* **71**: 747-758.

[19] Jurenka J., Spaniel M., 2014, Advanced FE model for simulation of pitting crack growth, *Advances in Engineering Software* **72**: 218-225.

[20] Glodez S., Ren Z., Flasker J., 1998, Simulation of surface pitting due to contact loading, *International Journal for Numerical Methods in Engineering* **43**: 33-50.

[21] Fajdiga G., Glodez Kramar, J., 2007, Pitting formation due to surface and subsurface initiated fatigue crack growth in contacting mechanical elements, *Wear* **262**: 1217-1224.

[22] Fajdiga G., Sraml M., 2009, Fatigue crack initiation and propagation under cyclic contact loading, *Engineering Fracture Mechanics* **76**: 1320-1335.

[23] Hannes D., Alfredsson B., 2013, Modelling of surface initiated rolling contact fatigue damage, *Procedia Engineering* **66**: 766-774.

[24] Hannes D., Alfredsson B., 2012, Surface initiated rolling contact fatigue based on the asperity point load mechanism - A parameter study, *Wear* **294**: 457-468.

[25] Davis J.R., 2005, *Gear Materials, Properties, and Manufacture*, ASM International, First Edition.

[26] Asi O., 2006, Fatigue failure of a helical gear in a gearbox, *Engineering Failure Analysis* **13**: 1116-1125.

[27] Moorthy V., Shaw B.A., 2012, Contact fatigue performance of helical gears with surface coatings, *Wear* **276-277**: 130-140.

[28] Budynas R.G., Nisbett J.K., 2011, *Shigley's Mechanical Engineering Design*, McGraw-Hill, New York.

[29] Abaqus/CAE User's Manual, Version 6.12, 2012.

[30] Rebbechi B., Oswald F.B., Townsend D.P., 1996, Measurement of gear tooth dynamic friction, *NASA Technical Report ARL-TR-1165*.

[31] Bomidi J.A.R., Sadeghi F., 2014, Three-demensional finite element elastic-plastic model for subsurface initiated spalling in rolling contacts, *Journal of Tribology* **136**: 011402-0114011.

[32] Juvinall R.C., Marshek K.M., 2012, *Fundamentals of Machine Component Design*, John wiley & sons, Hoboken.
[33] Johnson K.L., 1985, *Contact Mechanics*, Cambridge University Press, Cambridge.
[34] Richard H.A., Fulland M., Sander M., 2005, Theoretical crack path prediction, *Fatigue & Fracture of Engineering Materials & Structures* **28**: 3-12.
[35] Erdogan F., Sih G.C., 1963, On the crack extension in plates under plane loading and transverse shear, *Journal of Basic Engineering* **85**: 519-525.
[36] Hertzberg R.W., 1996, *Deformation and Fracture Mechanics of Engineering Materials*, John Wiley & Sons, New Jersey.
[37] Tanaka K., 1974, Fatigue crack propagation from a crack inclined to the cyclic tensile axis, *Engineering Fracture Mechanics* **6**: 493-507.